Application of the Voltage Control Technique and MPPT of Stand-alone PV System with Storage

Article *in* Advances in Electrical and Computer Engineering · February 2022

DOI: 10.4316/AECE.2022.01003

CITATION
1

READS
255

4 authors, including:

Jasna Hivziefendic
International BURCH University
46 PUBLICATIONS **107** CITATIONS
SEE PROFILE

Lejla Vuic
International BURCH University
11 PUBLICATIONS **102** CITATIONS
SEE PROFILE

Mirza Saric
JP Elektroprivreda BiH d.d. Sarajevo
58 PUBLICATIONS **189** CITATIONS
SEE PROFILE

Application of the Voltage Control Technique and MPPT of Stand-alone PV System with Storage

Jasna HIVZIEFENDIC[1], Lejla VUIC[1], Srdjan LALE[2], Mirza SARIC[1]
[1]*International Burch University, Sarajevo 71000, Bosnia and Herzegovina*
[2]*University of East Sarajevo, East Sarajevo 71123, Bosnia and Herzegovina*
lejla.vuic@ibu.edu.ba

***Abstract*—To provide a stable operation of a standalone microgrid based on the photovoltaic system in the most efficient way, various mechanisms and control strategies need to be engaged simultaneously. Modeling, simulation, and analysis of the microgrid system composed of PV generator, battery energy storage system (BESS), and DC/AC converter are presented in the paper. The PV generator operates in maximum power point (MPP) mode, while the BESS is deployed to enable power flow between the storage and consumers using the charge/discharge cycle of the battery. The maximum power point tracking (MPPT) control at the PV side, combined with battery control, is obtained by Perturb and observe (P&O) and Fuzzy Logic Control (FLC) algorithms. Simulation based voltage control strategy is performed by using both DC/DC buck-boost converter and DC/AC converter with aim to obtain stable voltage for different power inputs. Modeling and simulations are performed in MATLAB/Simulink software. It is demonstrated that proposed methods ensure a stable microgrid operation and PV system operation in MPP mode. Both MPPT algorithms, P&O and FLC, provided accurate responses with very high efficiency above 95%.**

***Index Terms*—battery management systems, fuzzy logic, maximum power point trackers, photovoltaic systems, voltage control.**

I. INTRODUCTION

The issues of climate change, environmental degradation and global requirements for carbon footprint reduction have shaped the framework for studying renewable energy sources (RES) and distributed generation (DG) grid integration. The application of RES, including solar energy and photovoltaic (PV) systems, is becoming an imperative and a driving force in development of smart grids. Additionally, the concept of microgrids is gaining worldwide attention due to its potential to contribute towards addressing and resolving some of the most important modern power system challenges. Standalone PV-based systems with storage can provide power for consumers in microgrids and can be more cost-effective when compared to traditional grid connection alternatives. Increased efficiency of power electronics devices additionally promotes the use of solar energy. Nevertheless, the large-scale integration of RES into power system causes numerous operational challenges such as voltage control, power system stability, and power quality [1]. In most cases, PV system grid integration requires voltage regulation to ensure stable system operation. Different voltage control methods based on DC/DC converters are presented in numerous research [1]. The microgrid voltage and frequency control strategy is analyzed in [2], describing the functioning and control of the inverter interface of DG. It is demonstrated that installation of DG in the power grid improves voltage profile by using an appropriate V-f control strategy and mechanism which are further applicable in the microgrid mode as well [3]. The traditional droop control method is proposed in [4].

Additional complexity of PV integration is triggered by inherent dependence on radiation intensity, which can cause low efficiency during the days with low radiations. Defining unique maximum power point (MPP) operation option is virtually impossible since the current – voltage curve in PV system is non-linear. The location of the peak power point is constantly varying with change of temperature and solar irradiance and is not known a priori [5]. Identifying peak power point on the I-V characteristic of the PV system to achieve a maximum power transfer is therefore essential. MPP can be positioned by applying maximum power point tracking (MPPT) algorithms, which have proven to be an effective instrument in obtaining the maximum output power while simultaneously increasing operational lifetime of PV systems [6]. Based on these facts, it can be concluded that MPPT algorithms remain an important part of PV system development and merit further attention.

Various MPPT algorithms are described in the literature [7-9]. The most extensively used algorithms include Incremental Resistance MPPT, Perturb and Observe (P&O) MPPT [10-12], Incremental Conductance (INC) MPPT, the Gradient Descent MPPT, Power Feedback MPPT, and Fuzzy Logic Control (FLC) [13–15]. More recent papers in this field with focus on MPPT algorithm performance highlight the importance and relevance and practical applicability of this research area. For example [16] presents a logarithmic Particle Swarm Optimization Global/Local MPPT for partially shaded PV systems and demonstrates the reduction of power oscillations during the search process as well as the faster convergence without the reduction of the search window. The most frequently researched topics are focused on the integration of the PV system into electrical grid and its functioning in the islanding mode.

Standalone PV system with storage and the assigned power electronic converters is designed, analyzed and tested in this article. Suggested standalone system is not connected on the electrical grid, so the main source of energy is PV system with battery energy storage system (BESS) as backup source. Major contribution of the presented research is visible in the coordination of various mechanisms and control strategies at the same time, such as voltage regulation at the inverter side, MPPT control of the PV system with aim to obtain the maximum output power and

battery charging/discharging control. By applying these control methods, the use of solar energy should be maximized in the most efficient way. Similarly, AC bus voltage stability is ensured for different modes of system operation. MPPT control is performed by applying two algorithms: P&O and FLC based MPPT algorithm. The proposed approach is tested, analyzed and confirmed on the real electrical distribution network model adjusted to operate in microgrid mode.

Remaining part of the paper is organized as follows: microgrid system configuration and modelling is described in the section 2 including PV and battery modelling together with voltage regulation and DC/AC converter; P&O and FLC based MPPT algorithms are presented in Section 3. Section 4 and 5 present the simulation results to validate the effectiveness of the implemented strategy and conclusions, respectively.

II. System Components and Modeling

The simple microgrid model composed of a PV system, BESS and AC loads, used as test model, is given on the Fig. 1. Two characteristics modes are analyzed in the research:

- Load is supplied only by the PV system;
- Load is supplied by the power from both, PV system and BESS.

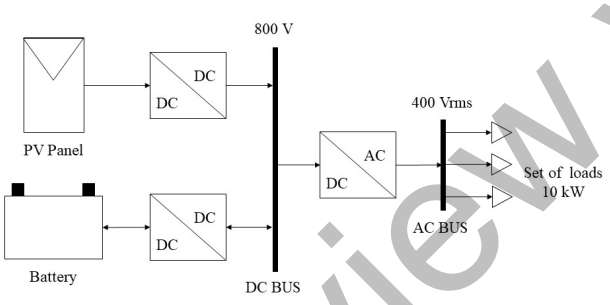

Figure 1. Microgrid configuration

In both cases, PV system operates in MPPT mode with aim to extract maximum power from solar energy. Analysis is performed for different input parameters for solar irradiation and temperature. For both modes, solar energy is used as the only power source, while battery serves as a backup power supply, which is also charged by solar energy, i.e., PV generator.

PV generator and storage battery are connected in parallel to DC side of the DC/AC interlinking converter, which is used for the voltage regulation of the load. On the DC side of the system, the PV generator is connected to DC/DC boost converter which controls power supplied by PV generator. In the case when the load is supplied only by PV system, load receives power generated by the PV generator through DC/AC inverter. The BESS is connected to DC side of the system by the bidirectional DC/DC buck-boost converter which is used for regulation of charging/discharging processes of batteries. Buck-boost converter can operate in two modes. When the PV system generates more power than load requires, excess power will be absorbed by the BESS, i.e., battery will be in the charging mode. In this case bidirectional converter operates in buck mode and controls charging battery current. If the power generated by the PV system is not sufficient, BESS serves as a backup power supply. In this case bidirectional converter operates in boost mode and at the same time regulates voltage on DC side. Hence, battery operates in discharging mode. The model of the system modeled in the Simulink is given on the Fig. 2.

The DC bus voltage is maintained within permissible limits by the combination of PV system and BESS, through the regulation of power unbalance created by load and the variation of the source. Under this condition, the charging procedure of the BESS requires to be controlled, as the charge current or charge voltage of the battery can reach the maximum values given by the manufacturers. Research in the paper is focused on the coordination control between the boost converter at PV side and buck-boost converter at BESS side together with DC/AC interlinking inverter.

A. PV System

PV cell can be modeled in several ways. The most frequently used models consist of current source connected in parallel with p-n diodes. Since there is no ideal solar cell, parallel and series cell resistance are taken into consideration as well. R_p, parallel resistance, is a path with high conductivity across the p-n junction, while R_s, serial resistance, represents the sum of resistances of bulk and diffused layer on top and the contact resistances on the front and back surfaces of PV array. Current of PV cells, I_C, can be represented as follows:

$$I_c = I_{ph} - I_d - \frac{V + R_s \cdot I_c}{R_p} \tag{1}$$

where, I_{ph} is the photocurrent produced for given insolation conditions, I_d – diode current, V – PV cell voltage.

Relationship between diode current and voltage is given as:

$$I_d = I_0 \left(e^{\frac{q \cdot V}{A \cdot k \cdot T_c}} - 1 \right) \tag{2}$$

where, q is the electron charge, k is Boltzmann's constant (1.38 · 10-23 J/K), T_c is absolute PV temperature, A is ideality factor, and I_0 is inverse saturation current which depends on the temperature.

The output current of PV array consisted of series (n_s) and parallel (n_p) connected cells is directly proportional to the inverse saturation current I_0 and is calculated according to the equation (3). Both currents, I_d and I_0, depend on irradiance and the temperature levels.

$$I_d = n_p I_0 \left(e^{\frac{q(V + R_s \cdot I)}{n_s \cdot A \cdot k \cdot T_c (1 - b_t (T_c - T_n))}} - 1 \right) \tag{3}$$

where, T_n is the nominal temperature and b_t is the voltage temperature coefficient.

The photocurrent depends on solar irradiation level G and the temperature, and it is defined by the equation (4):

$$I_{ph} = I_n \left(1 + a_k \left(T_c - T_n\right)\right) \frac{G}{1000} \tag{4}$$

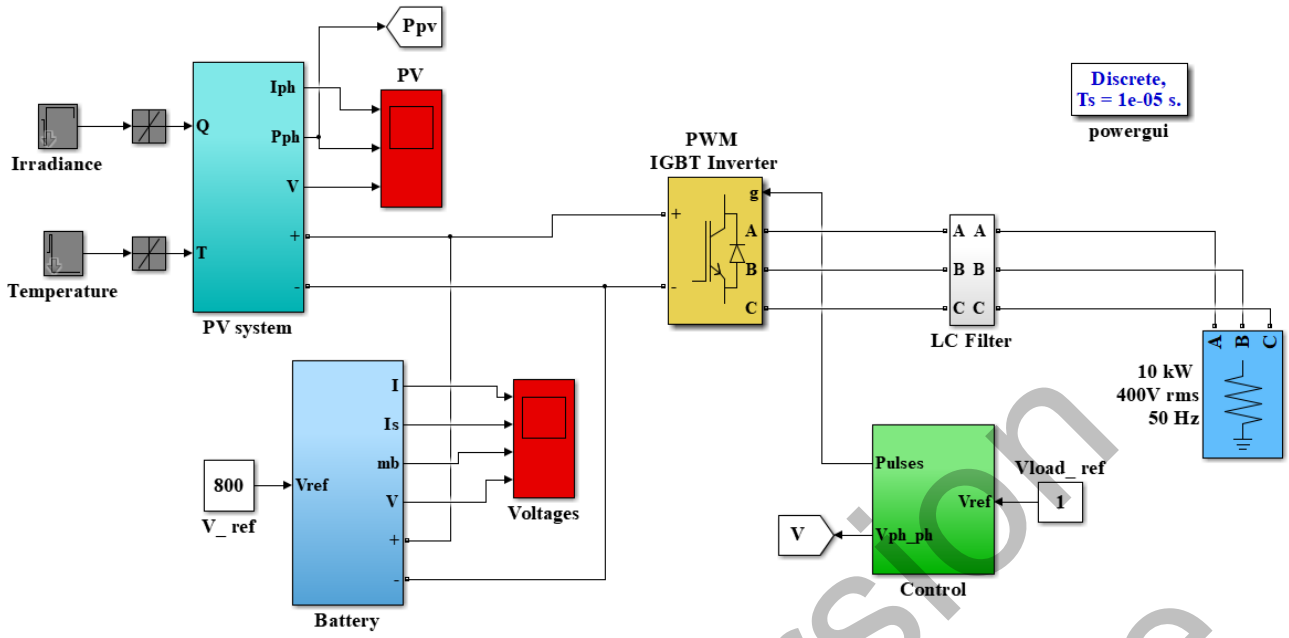

Figure 2. Structure of the microgrid modeled in Simulink

where, I_n is the photocurrent under nominal conditions, and a_k is the current temperature coefficient.

B. Battery Modeling

The processes of charging/discharging the battery storage with buck-boost converter and PI regulators are simulated in MATLAB/Simulink. Model of the BESS is presented in the Fig. 3.

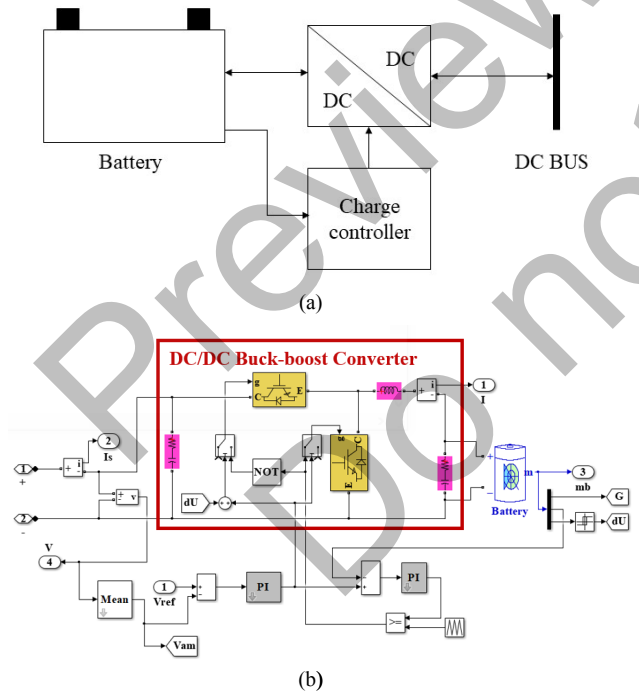

Figure 3. The battery storage with buck-boost converter: a - Block diagram; b - Model in Simulink

The battery is connected on the DC side through bidirectional DC/DC buck-boost converter. One of the constraints related to the battery functioning is capacity limit, which is measured by the state of charge (SOC) parameter, which prevents batteries from undercharging and overcharging [17]. It is defined as follows:

$$SOC(t) = \frac{Q(t)}{Q_n} \tag{5}$$

where, Q is defined as current capacity of the battery (Ah) and Q_n as the nominal capacity of the battery (Ah) given by manufacturer.

Charging and discharging processes of the lead-acid battery used for research, are modeled with the equations (6) and (7).

$$V_{batt} = V_0 - R*i - K\frac{Q}{Q - i_t}\left(i_t + i^*\right) + e^t \tag{6}$$

$$V_{batt} = V_0 - R*i - \left[K\frac{Q}{i_t - 0.1Q}\right]i^* - \left[K\frac{Q}{Q - i_t}\right]i_t + e^t \tag{7}$$

Battery voltage depends on Q, constant battery voltage V_0, internal resistance R, battery current i, polarization resistance K, actual charge of battery i_t and filtered current i^*. A two-loop control scheme, based on inner and outer PI controllers, maintains the DC bus voltage (V_{DC}) in predefined voltage range [18]. Reference voltage used in the outer control loop is the operational voltage of DC bus and it has value of 800 V. This reference voltage and the instantaneous voltage of DC bus are input signals for the outer PI controller. The output of the PI controller generates reference input for the inner control loop. Comparing the measured battery output current and the reference current, error signal, that is input of inner PI regulator, will be generated. If there is a difference between V_{DC} and reference voltage, the outer control loop generates the reference current that will ensure charging/discharging of the battery. If the difference is positive, the inner control loop will charge the battery. DC bus voltage will be decreased to the reference value as the surplus of the power is absorbed by the battery. If the reference voltage is lower than the V_{DC}, the output of the outer control loop will be the current with opposite direction and the inner control loop will discharge the battery. This process is further regulated by the battery capacity.

C. Voltage Regulation with DC/AC Inverter

For islanded mode of operation, the BESS regulates V_{DC} while the DC/AC inverter is responsible for maintaining a stable voltage on the AC side of the system [19]. The converter that connects the DC and AC side of the system is operated using the control signals provided by the algorithm used for load voltage regulation.

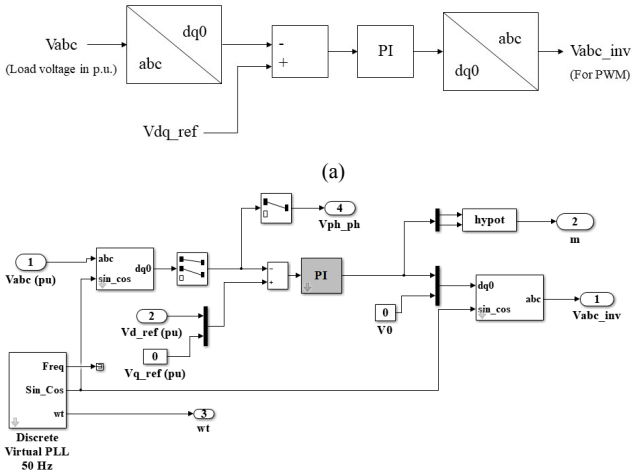

Figure 4. Load voltage control loop: a - Block diagram; b - Model in Simulink

Fig. 4a shows the block diagram of the load voltage control loop, while Fig. 4b presents its model in Simulink. The reference voltage is compared with measured three-phase load voltage and the obtained difference is used as the input variable of the PI controller. The Park transformation is applied to the three-phase load voltage prior to measurement of the PI input variable. The duty cycle, i.e., *d* and *q* components are the outputs of the PI controller and subject to the inverse Park transformation to obtain a real value of three-phase voltage. Moreover, the PWM pulses that drive DC/AC interlinking converter, are generated from *d* and *q* components.

III. MPPT ALGORITHMS

To obtain maximum power from PV system, load must be continuously adapted to the PV operating point. MPP is dynamically changing due to variations in ambient temperature and solar radiations. Therefore, MPP must be searched by MPPT controllers. DC/DC or DC/AC converters are installed between the PV modules and loads with aim to continuously track MPP of the PV modules and adjust the load to their operational characteristics. The role of the DC/DC boost converter, used in the research, is to step-up the DC voltage generated from the PV system, for given irradiation and temperature conditions [20]. The proposed PV system with boost converter is given in Fig. 5. The measured output voltage and current of the PV array are used as inputs for DC/DC boost converter, as shown on block diagram in Fig. 6. By finally, P&O and FLC algorithms are used for MPPT in this paper.

A. Perturb and Observe (P&O) Algorithm

P&O algorithm is classified as direct method based on the constant disturbance of the operating point position of the PV array with the aim of bringing it closer to the MPP.

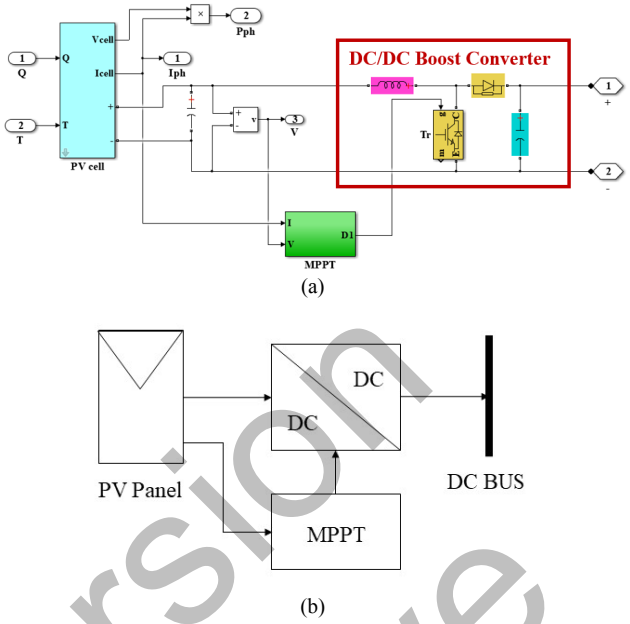

Figure 5. PV system: a - Block diagram; b - Model in Simulink

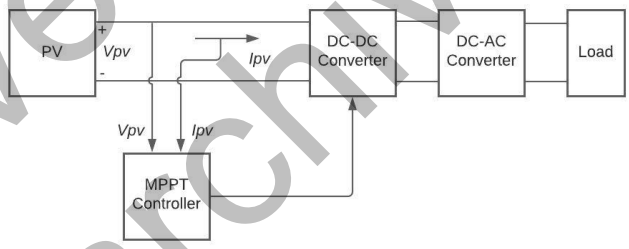

Figure 6. The block diagram of the MPPT control

The result of the P&O algorithm is the value of the duty cycle D, by which the operation of the boost converter is regulated. The load curve, which intersects the V-I curve of the PV array to obtain the operating point, depends on the obtained duty cycle:

$$I = \frac{1}{R_0}\left(\frac{1}{1-D}\right)^2 V \tag{8}$$

where, R_0 is the load resistance.

By adjusting the duty cycle, the operating point will slide on the I-V characteristics of the PV array. A constant update of the duty cycle value has to be done to bring the operating point to the position of the MPP.

At instant kΔT, where ΔT is the period of the update of D, the value of the instantaneous PV output power is obtained by the measurement of its current and voltage. That power is further compared to power obtained in the previous moment (k-1)ΔT. The analysis of the change in output power, resulting from the change in voltage, is performed. Depending on the sign of the change in power and voltage, the duty cycle increases or decreases by a predefined value ΔD. The described procedure is constantly repeated and at some instant, the operating point will come very close to the point of maximum power [21-22]. The flowchart of the P&O algorithm is presented in Fig. 7.

The nature of the P&O technique is such that the operating point constantly oscillates around the MPP of the solar array. The most important parameter that affects the

efficiency of the P&O method is the perturbation step of the converter duty cycle, which directly affects the step of the voltage change. With a small step, it is possible to achieve great precision at operating point, at the cost of slow response to changes in maximum power due to variations in temperature and solar irradiance. In the case of a large perturbation step, the algorithm will react quickly to changes, but at the cost of significant deviations in the operating point.

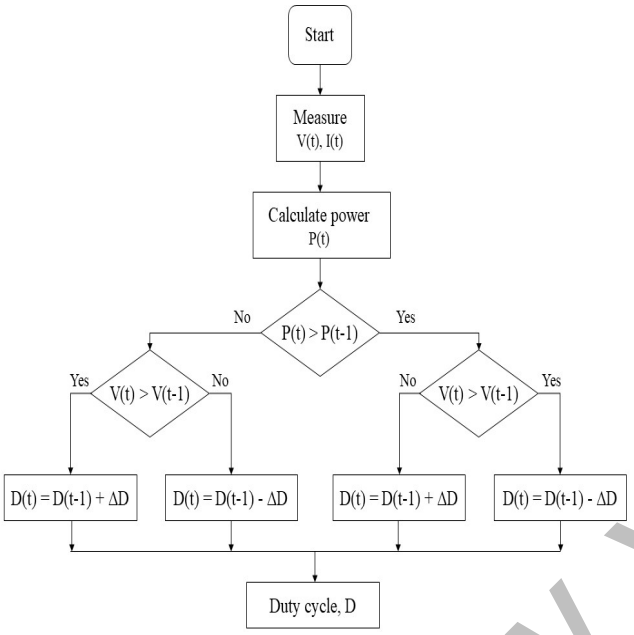

Figure 7. The flowchart of the P&O algorithm

The perturbation step used in this paper is constant and has value of 0.001. The model of the P&O algorithm in the Simulink is presented in Fig. 8.

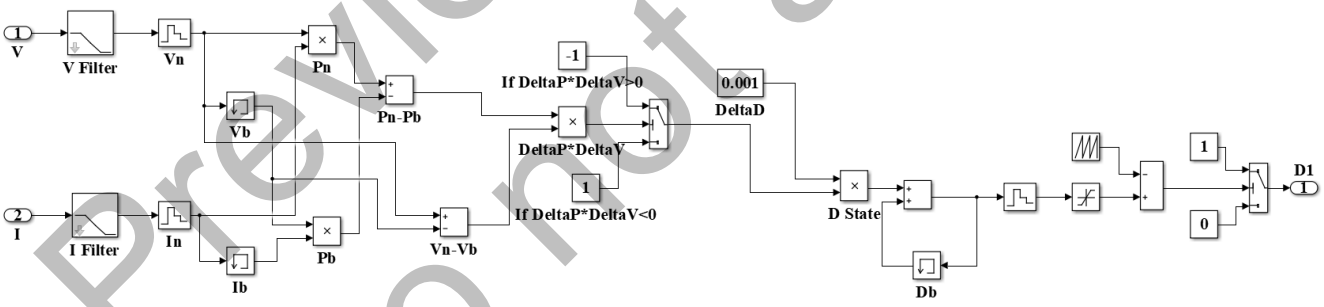

Figure 8. Simulink model of the P&O algorithm

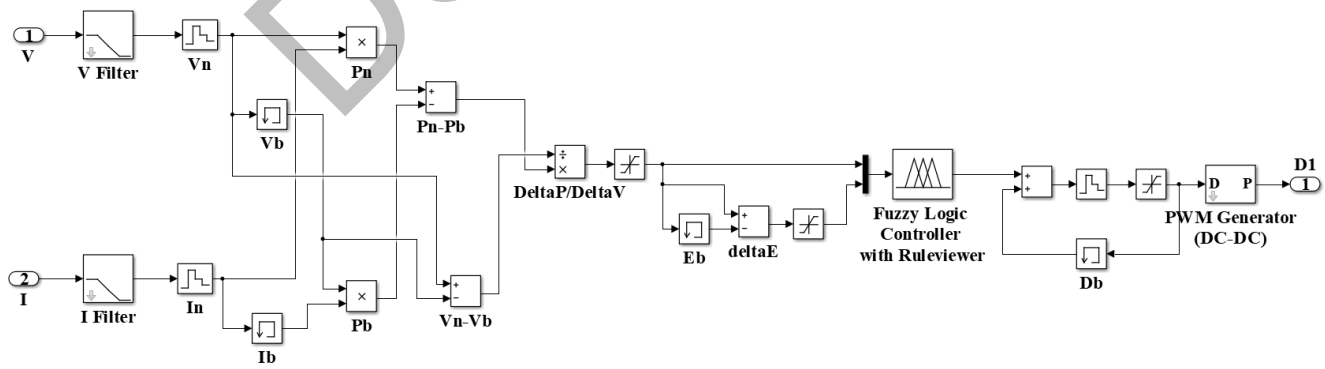

Figure 9. FLC based MPPT algorithm in Simulink

Fuzzy system consists of 3 stages: fuzzification, inference and defuzzification. Membership functions (MF) that are defined in fuzzification stage are represented using fuzzy triangular function with seven membership functions

B. Fuzzy Logic Control (FLC) Algorithm

PV system is a major source of uncertainties due to the inherent properties of solar irradiation. One possible approach of addressing these uncertainties is the application FLC for MPPT algorithm due to its independence of mathematical models. FLC can also operate with imprecise inputs and can handle nonlinearity [23].

Proposed FLC model, shown in Fig. 9 has two input variables. The first one is the signal error E, which represents a change in active power P and voltage V. The second is the difference between two consecutive instances of measurement, i.e., change of error, dE. The aim of the FLC based MPPT is to obtain a change in the PV voltage as a function of the duty cycle (D), which is the output of FLC.

$$E(k)=\frac{\Delta P}{\Delta V}=\frac{P(k)-P(k-1)}{V(k)-V(k-1)} \tag{9}$$

$$dE(k)=E(k)-E(k-1) \tag{10}$$

In Table I, four different operating principles of the FLC are presented. Different changes in power (ΔP) and voltage (ΔV) result in different actions that should be applied to the voltage (V) of the PV system.

TABLE I. OPERATING PRINCIPLES OF FLC

ΔP	ΔV	
ΔP > 0	ΔV > 0	V is increased
ΔP > 0	ΔV < 0	V is decreased
ΔP < 0	ΔV > 0	V is decreased
ΔP < 0	ΔV < 0	V is increased

(levels): NB (Negative Big), NM (Negative Medium), NS (Negative Small), ZE (Zero), PS (Positive Small), PM (Positive Medium) and PB (Positive Big). The MFs used for the inputs and output are presented in Fig. 10. When inputs are fuzzified the inference engine processes them using the rule base presented in Table II.

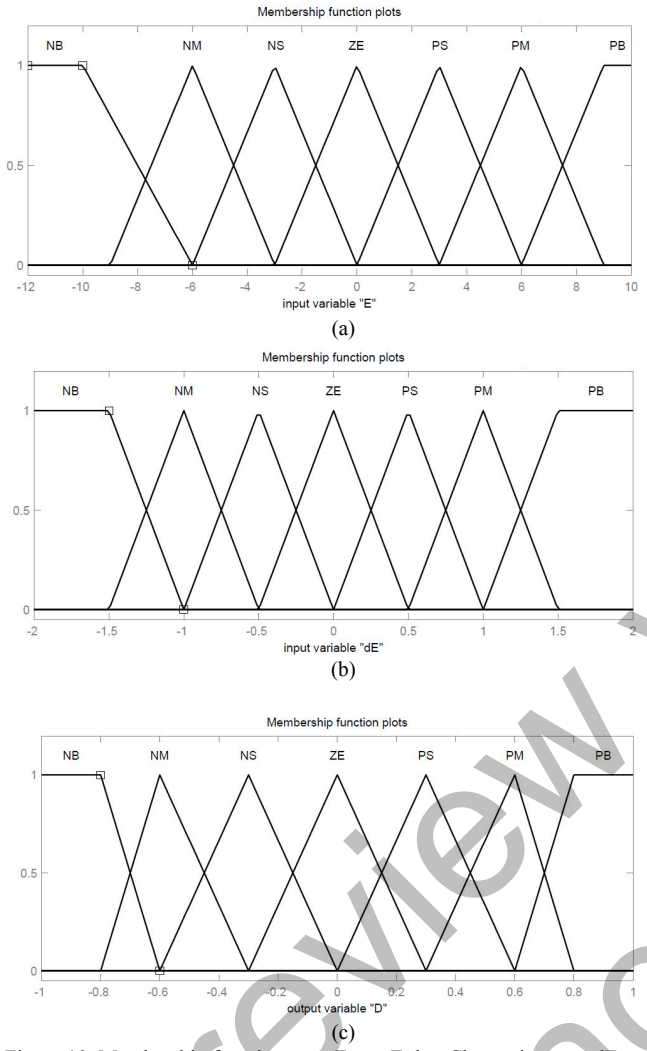

Figure 10. Membership functions: a – Error, E; b – Change in error, dE; c – Duty cycle, D

IV. Results and Discussion

A set of the loads from the 10/0.4 kV test system, modeled as a single equivalent load, are used to verify the proposed MPPT and voltage regulation concept. The total power requirement of the real system used in the paper is 0.663 MVA including 0.629 MW of the real power and 0.210 MVAr of the reactive power.

System analysis is carried out in Simulink with the Simscape power systems toolbox. The proposed microgrid model is presented in the Fig. 2. It is composed of the PV generator and BESS on DC side and 3-phase 10 kW load on the AC side. The PV array parameters given in Table III are obtained for the standard test conditions, i.e., for solar irradiance of 1000 W/m^2 and temperature of 25□. The open circuit voltage (V_{OC}) of the array is 310.83 V, while the short circuit current (I_{SC}) is 64.24 A. The maximum power of the considered PV system is 14.75 kW. Parameters of the storage battery are chosen to compensate the output power of PV generator when the level of irradiance is low. Nominal battery voltage is 400 V while its rated capacity is 30 Ah. It is presupposed that the battery is fully charged at the initial point. The V_{DC} of 800 V is regulated with both DC/DC boost converter integrated in the PV system and DC/DC buck-boost converter from the BESS.

Table II. Rule Base for FLC

E/dE	NB	NM	NS	ZE	PS	PM	PB
NB	ZE	ZE	ZE	PB	PM	PM	PB
NM	NS	ZE	ZE	PB	PM	PM	PM
NS	ZE	PS	ZE	NS	PS	PM	PM
ZE	PS	PS	ZE	ZE	ZE	NS	NS
PS	NM	NM	NS	NS	ZE	ZE	ZE
PM	NM	NM	NM	NM	ZE	ZE	ZE
PB	NB	NB	NB	NB	ZE	ZE	ZE

Table III. Simulation Parameters of the PV Array

Parameter	Symbol	Value
Maximum power	P_{MPP}	14.75 kW
Voltage at maximum power	V_{MPP}	249 V
Current at maximum power	I_{MPP}	59.24 A
Open circuit voltage	V_{OC}	310.83 V
Short circuit current	I_{SC}	64.24 A

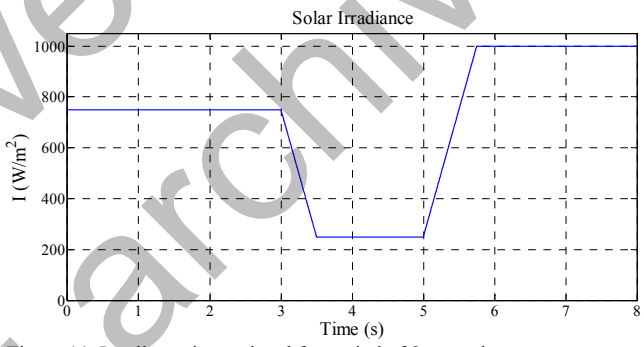

Figure 11. Irradiance input signal for period of 8 seconds

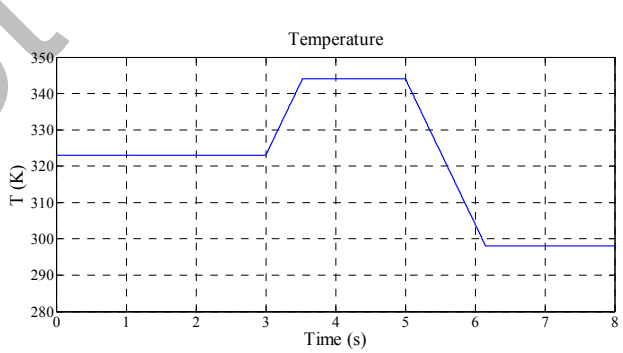

Figure 12. Temperature input signal for period of 8 seconds

The analysis is performed for different inputs parameters of solar irradiance and temperature. Solar irradiance has been changing in the range from 250 W/m^2 to 1000 W/m^2 while the temperature has been varied from 298 to 344 K (25□ to 70□). For the first 3 seconds, solar irradiance is 750 W/m^2 and the temperature is 323 K (50□), after which they are changed to 250 W/m^2 and 344 K (70□). At 5 s, the solar irradiance jumps to 1000 W/m^2 and the temperature drops to 298 K (25□). These inputs to the system are presented in Fig. 11 and Fig. 12.

A. MPPT Simulation Results

MPPT simulation results are obtained by applying two

algorithms: P&O and FLC based algorithm. The PV output power is analyzed for the cases when the irradiance and the temperature are 1000 W/m^2 and 298 K (25□), 750 W/m^2 and 323 K (50□), and 250 W/m^2 and 344 K (70□). The PV current and voltage are input signals for both MPPT algorithms.

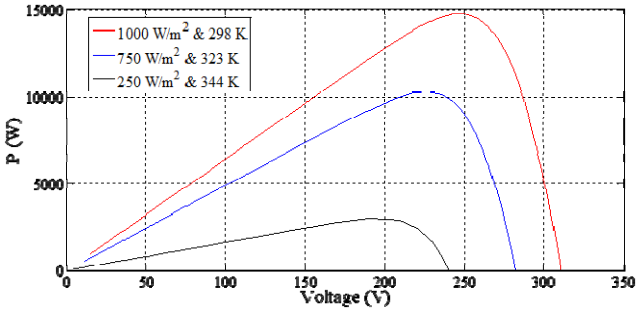

Figure 13. P-V characteristic for various weather conditions

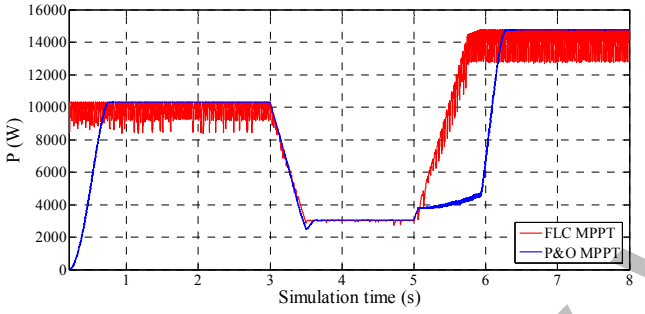

Figure 14. The PV output power obtained with MPPT algorithms

Fig. 13 presents the P-V characteristic for different illumination density. In the case when the irradiance is 1000 W/m^2 and temperature is 25□ (298 K), the maximum power output of the array is 14.75 kW. Moreover, the power given by the array is 10.3 kW when there is 750 W/m^2 of irradiance and 50□ (323 K) of temperature. When the irradiance and temperature are 250 W/m^2 and 70□ (344 K), respectively, the power output of the array is minimum, and its value is 3 kW. It is shown that PV array has lower power output at lower irradiance and higher temperatures.

Generated output power for both algorithms is presented in the Fig. 14. Blue line indicates P&O while red line represents the FLC based MPPT algorithm. The values obtained for each algorithm are equivalent to the values obtained from the P-V characteristic for various irradiance and temperature values. During the first 3 s, the output of the PV system is 10.29 kW. For irradiance of 250 W/m^2 and temperature of 70□ (344 K), its power output drops to 3 kW. However, when temperature drops to 25□ and the irradiance increases to 1000 W/m^2, the PV system's output power jumps to 14.74 kW. Therefore, the effectiveness of the MPPT algorithms' performance has been confirmed.

It is visible from the Fig. 14 that the FLC based MPPT algorithm better adapts to the variations of the illumination intensity than P&O algorithm. On the beginning of simulation and at 5 s transition time, FLC algorithm, tracks the MPP immediately, while the P&O algorithm has some delay. In other words, it has higher response time.

Comparison of the efficiency of the proposed MPPT algorithms with algorithms from recent research papers is presented in Table IV. In the existing literature most of the simulation results are obtained in different environmental conditions and capacity. Algorithms used in this paper have the efficiency of 98 % in the system used, which is better than efficiencies of the other algorithms used for different systems. This once more proves the applicability of the proposed algorithms.

TABLE IV. COMPARISON OF MPPT ALGORITHMS

	Used algorithms	**Efficiency**
This paper	P&O FLC	97.9 % 98 %
Reference [24] with fixed irradiance	FLC	94.8 %
Reference [24] with partial shading	FLC	97.8 %
Reference [25] with fixed irradiance	P&O	97 %
Reference [25] with partial shading	P&O	75 %
Reference [26]	P&O	97.8 %

B. Voltage Regulation Simulation Results

Voltage regulation of the system has been analyzed for the DC and the AC side separately. As it is illustrated in Fig. 4, the MPPT methods operate with the use of the boost converter which transfers the maximum PV power to the DC-link by regulating the PV voltage. At the same time, voltage on the DC-link is controlled by the BESS which enables power balance at the DC side of the considered system.

Fig. 15 presents the SOC of the battery from the used system. During the first 3 seconds, the PV array produces 10.3 kW which is not enough for the load. Therefore, the battery starts to discharge to provide required power to the load. For the next two seconds, the generated power generated from the PV array is decreased to 3 kW which causes the battery to discharge more. When simulation reaches 5 seconds, the PV array starts to generate power which is sufficient for the load. Therefore, the discharging of the battery stops, and its SOC remains at the same level. Due to the different response times of the MPPT algorithms there is a quite small difference between SOC with P&O and SOC with FLC algorithm, which can be seen on Fig. 15.

Besides the battery charging/discharging regulation, the DC/DC buck-boost converter is responsible for the regulation of the DC bus voltage. Fig. 16 shows that the DC bus voltage is maintained at the constant desired value of 800 V. Therefore, the efficiency of the control of the converter has been confirmed.

The DC/AC interlinking converter regulates the voltage at the AC side of the system. Magnitudes of the voltages on the AC side for the P&O algorithm are shown in Fig. 17a. The first graph presents the inverter's line voltage.

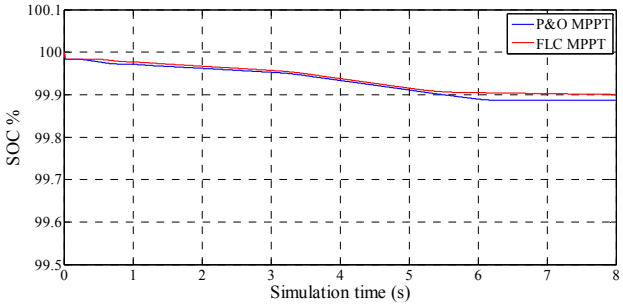

Figure 15. SOC of the battery

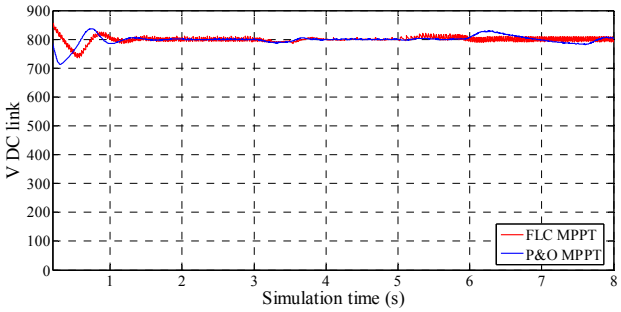

Figure 16. DC bus voltage

The load line voltage is presented on the second graph, while the amplitude of the load voltage in p.u. is given in third graph. The fourth graph presents the three-phase load voltage. Voltages on the AC side have same waveforms for the FLC based MPPT algorithm, as well. For clear and concise analysis, waveforms obtained using only P&O algorithm are used.

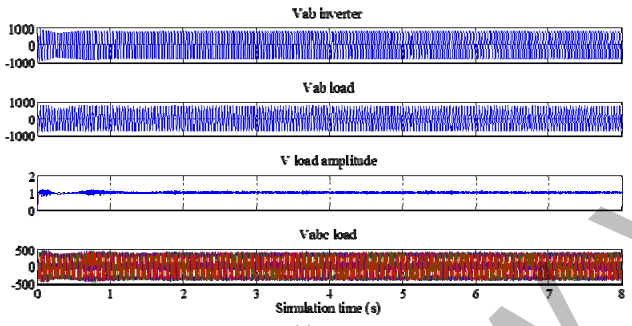

(a)

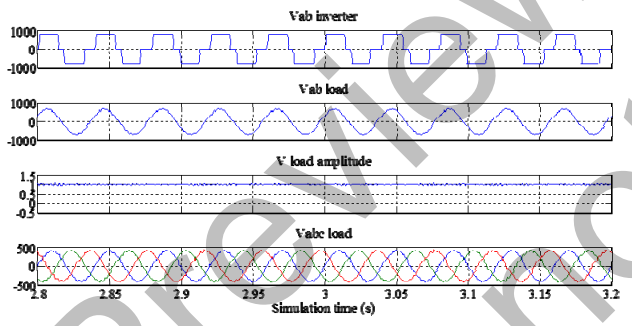

(b)

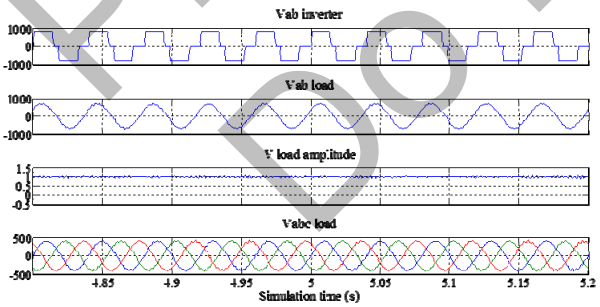

(c)

Figure 17. Load voltage regulation: a - Load voltages during simulation; b- Load voltages at transition time 3 s; c - Load voltages at transition time 5 s DC bus voltage

For the analysis of load voltage regulation, transition times t = 3 s, and t = 5 s are observed. Fig. 17b and Fig. 17c show that there is no deviation in load voltage, during these transitions. The load voltage amplitude has been maintained the range of 0.95 to 1.05 p.u.

C. Step Load Response

The performance and efficiency of the proposed voltage regulation method is analyzed for different values of the load. It is defined that the simulation lasts for 10 s. At 6.5 s the change of the load from 10 kW to 20 kW is introduced, by inserting additional load. This change lasts for 1 s. At 7.5 s additional load is disconnected and the value of the load is returned to 10 kW.

The amplitude of the load voltage is analyzed in per unit system, with the base voltage of 400 V. The behavior of voltage is represented in the Fig. 18. It is obvious that the value of the voltage is affected by the load change. However, this change lasts only for 0.5 s, whereupon the voltage value returns to acceptable range. When the value of the load is returned to 10 kW, load voltage adapts to change and keeps the magnitude within prescribed range.

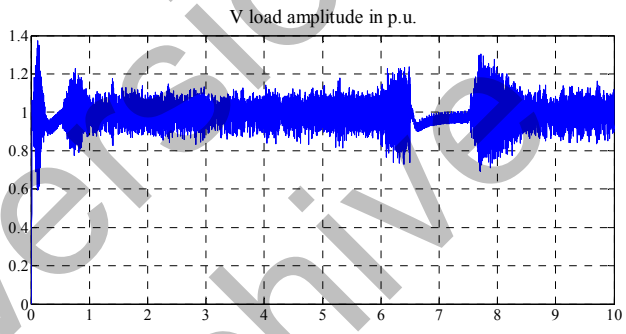

Figure 18. Voltage at the load side when the load is changed

Fig. 19 represents the SOC of the battery for the case when the change of load occurs. For the first 6 s, the SOC is the same as it was in the case when the regular load was present in the system. After 6.5 s, additional discharge of the battery has occurred due to increase in the load. For the last 2.5 s of the simulation, SOC maintains previously obtained value, as the PV system generate sufficient power for the load.

It is shown that suggested system will remain stable under different required conditions. Voltage and the current of the PV system will be affected by changing the temperature and irradiance and it can further influence to the output voltage stability. However, the voltage stability is insured by the BESS application in the system.

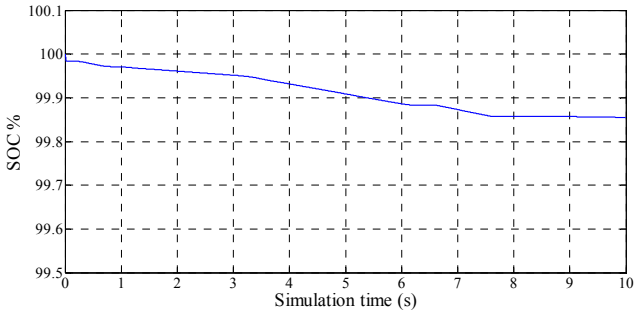

Figure 19. SOC of the battery when the load is changed

Furthermore, there is decrease in the output voltage caused by the load changes in the system that last for a very short period (0.5 s). However, voltage control is provided by the PI controller which maintain voltage parameters in

defined range.

The research results presented in this paper contain information that can be used in practical situations to design and operate realistic microgrids. However, the list of realistic problems faced by microgrids are by no means exhausted by the results presented in this paper. This fact paves a path for interesting future work, which is related to these results. For example, present research can be extended to include consideration of frequency control strategy. Also, further hardware extensions are planned in the laboratory in order to provide more results and experimental validations in this field. Further, the field of MPPT algorithms is continuously evolving, which makes the design and implementation of new MPPT algorithms a promising research direction. Also, an extension of the existing generation capability with new renewable technologies, such as wind, is an important future research direction. Finally, some of the problems related to continuous operation of similar systems will inevitably be subjected to inherent problems caused by constant load and production variation. Therefore, some type of generation based on traditional electrical energy generation technologies, such as diesel generator, should be considered as a possible system extension.

V. Conclusion

In this paper, voltage control method of a stand-alone AC/DC microgrid system composed of PV generator, BESS and DC/AC converter is analyzed. In the proposed test system, PV generator operates in MPP mode, while the storage unit is deployed to enable power flow between the storage and consumers. P&O and FLC based algorithms are used for MPPT control to obtain and maintain the maximum generated power from the PV array via DC/DC boost converter for various weather conditions. The simulation results show that FLC based algorithm achieves better response time for reaching MPP than P&O algorithm. However, both algorithms provided accurate responses with very high efficiency. The voltage control method on the DC side is obtained using DC/DC buck-boost converter. Output voltage on the AC link is controlled by DC/AC converter. It is shown that the load voltage remains within allowed limits, even with different power inputs in the system. The simulation results show that the proposed microgrid operates in stable mode for different illumination and temperature intensities. The presented strategy ensures simultaneous operation of MPPT, BESS and DC/AC converter providing the maximum power from PV system and voltage stability.

Future research pathway of this paper includes the integration of the backup diesel generator to the proposed microgrid model in order to design and investigate the performance of Voltage-frequency (V-f) control algorithm. Additionally, future research directions will focus on design, implementation, and testing of the MPPT algorithms based on various computational intelligence tools.

References

[1] L. Bandic, J. Hivziefendic, M. Saric, and M. Tesanovic, "Voltage regulation of PV system with MPPT and battery storage in microgrid," in 2020 International Conference on Smart Systems and Technologies (SST), Osijek, Croatia, Oct. 2020, pp. 161–166. doi:10.1109/SST49455.2020.9264071

[2] S. Adhikari and F. Li, "Coordinated V-f and P-Q control of solar photovoltaic generators with MPPT and battery storage in microgrids," IEEE Trans. Smart Grid, vol. 5, no. 3, pp. 1270–1281, May 2014. doi:10.1109/TSG.2014.2301157

[3] M. Šarić, J. Hivziefendić, and L. Bandić, "Analysis and control of DG influence on voltage profile in distribution network," in M. Hadžikadić and S. Avdaković, (Eds) Advanced Technologies, Systems, and Applications II, vol. 28, Cham: Springer International Publishing, 2018, pp. 30–43. doi:10.1007/978-3-319-71321-2_3

[4] J. C. Vasquez, R. A. Mastromauro, J. M. Guerrero, and M. Liserre, "Voltage support provided by a droop-controlled multifunctional inverter," IEEE Trans. Ind. Electron., vol. 56, no. 11, pp. 4510–4519, Nov. 2009. doi:10.1109/TIE.2009.2015357

[5] H. Bounechba, A. Bouzid, H. Snani, and A. Lashab, "Real time simulation of MPPT algorithms for PV energy system," Int. J. Electr. Power Energy Syst., vol. 83, pp. 67–78, Dec. 2016. doi:10.1016/j.ijepes.2016.03.041

[6] A. Ravi1, J. Shameema Sulthana, R. Satheesh, and R. Aandal, "Conventional maximum power point tracking techniques for solar photo voltaic systems: A concise review," J. Crit. Rev., vol. 7, no. 06, Apr. 2020. doi: 10.31838/jcr.07.06.18

[7] Y.-H. Liu, J.-H. Chen, and J.-W. Huang, "A review of maximum power point tracking techniques for use in partially shaded conditions," Renew. Sustain. Energy Rev., vol. 41, pp. 436–453, Jan. 2015. doi:10.1016/j.rser.2014.08.038

[8] S. Motahhir, A. El Hammoumi, and A. El Ghzizal, "The most used MPPT algorithms: Review and the suitable low-cost embedded board for each algorithm," J. Clean. Prod., vol. 246, p. 118983, Feb. 2020. doi:10.1016/j.jclepro.2019.118983

[9] P. Mittal, T. Goel, and P. Gupta, "Evolution of MPPT algorithms in solar arrays," Mater. Today Proc., vol. 37, pp. 3154–3158, 2021. doi:10.1016/j.matpr.2020.09.045

[10] S. Lyden and M. E. Haque, "Maximum Power Point Tracking techniques for photovoltaic systems: A comprehensive review and comparative analysis," Renew. Sustain. Energy Rev., vol. 52, pp. 1504–1518, Dec. 2015. doi:10.1016/j.rser.2015.07.172

[11] N. S. Jayalakshmi, D. N. Gaonkar, S. Adarsh, and S. Sunil, "A control strategy for power management in a PV-battery hybrid system with MPPT," in 2016 IEEE 1st International Conference on Power Electronics, Intelligent Control and Energy Systems (ICPEICES), Delhi, India, Jul. 2016, pp. 1–6. doi:10.1109/ICPEICES.2016.7853112

[12] S. A. Oliveira da Silva, L. P. Sampaio, F. Marcos de Oliveira, and F. R. Durand, "Feed□forward DC□bus control loop applied to a single□phase grid□connected PV system operating with PSO□based MPPT technique and active power□line conditioning," IET Renew. Power Gener., vol. 11, no. 1, pp. 183–193, Jan. 2017. doi:10.1049/iet-rpg.2016.0120

[13] E. Radwan, M. Nour, E. Awada, and A. Baniyounes, "Fuzzy logic control for low-voltage ride-through single-phase grid-connected PV Inverter," Energies, vol. 12, no. 24, p. 4796, Dec. 2019. doi:10.3390/en12244796

[14] J. P. Ram, T. S. Babu, and N. Rajasekar, "A comprehensive review on solar PV maximum power point tracking techniques," Renew. Sustain. Energy Rev., vol. 67, pp. 826–847, Jan. 2017. doi:10.1016/j.rser.2016.09.076

[15] D. Haji and N. Genc, "Fuzzy and P&O based MPPT controllers under different conditions," in 2018 7th International Conference on Renewable Energy Research and Applications (ICRERA), Paris, Oct. 2018, pp. 649–655. doi:10.1109/ICRERA.2018.8566943

[16] S. Makhloufi and S. Mekhilef, "Logarithmic PSO based global/local maximum power point tracker for partially shaded photovoltaic systems," IEEE J. Emerg. Sel. Top. Power Electron., pp. 1–1, 2021. doi:10.1109/JESTPE.2021.3073058

[17] O. Tremblay and L.-A. Dessaint, "Experimental validation of a battery dynamic model for EV applications," World Electr. Veh. J., vol. 3, no. 2, pp. 289–298, Jun. 2009. doi:10.3390/wevj3020289

[18] P. Wang, C. Jin, D. Zhu, Y. Tang, P. C. Loh, and F. H. Choo, "Distributed control for autonomous operation of a three-port AC/DC/DS hybrid microgrid," IEEE Trans. Ind. Electron., vol. 62, no. 2, pp. 1279–1290, Feb. 2015. doi:10.1109/TIE.2014.2347913

[19] J. Hu, Y. Shan, Y. Xu, and J. M. Guerrero, "A coordinated control of hybrid ac/dc microgrids with PV-wind-battery under variable generation and load conditions," Int. J. Electr. Power Energy Syst., vol. 104, pp. 583–592, Jan. 2019. doi:10.1016/j.ijepes.2018.07.037

[20] S. E. Babaa, G. E. Murr, F. Mohamed, and S. Pamuri, "Overview of boost converters for photovoltaic systems," J. Power Energy Eng., vol. 06, no. 04, pp. 16–31, 2018. doi:10.4236/jpee.2018.64002

[21] B. Das, A. Jamatia, A. Chakraborti, P. R. Kasari, and M. Bhowmik, "New Perturb and Observe MPPT algorithm and its validation using data from PV module," vol. 4, no. 1, p. 13

[22] A. Škamo, M. Šarić, and L. Vuić, "Comparison of different maximum power point tracking algorithms," in Advanced Technologies, Systems, and Applications VI, vol. 316, N. Ademović, E. Mujčić, Z. Akšamija, J. Kevrić, S. Avdaković, and I. Volić, Eds. Cham: Springer International Publishing, 2022, pp. 117–132. doi:10.1007/978-3-030-90055-7_10

[23] M. N. Ali, K. Mahmoud, M. Lehtonen, and M. M. F. Darwish, "Promising MPPT methods combining metaheuristic, fuzzy-logic and ANN techniques for grid-connected photovoltaic," Sensors, vol. 21, no. 4, p. 1244, Feb. 2021. doi:10.3390/s21041244

[24] U. Yilmaz, A. Kircay, and S. Borekci, "PV system fuzzy logic MPPT method and PI control as a charge controller," Renew. Sustain. Energy Rev., vol. 81, pp. 994–1001, Jan. 2018. doi:10.1016/j.rser.2017.08.048

[25] M. S. Nkambule, A. N. Hasan, and A. Ali, "MPPT under partial shading conditions based on Perturb & Observe and Incremental Conductance," in 2019 11th International Conference on Electrical and Electronics Engineering (ELECO), Bursa, Turkey, Nov. 2019, pp. 85–90. doi:10.23919/ELECO47770.2019.8990426

[26] A. A. E. B. A. E. Halim, N. H. Saad, and A. A. E. Sattar, "Application of a combined system between Perturb and Observe method and Incremental Conductance technique for MPPT in PV systems," in 2019 21st International Middle East Power Systems Conference (MEPCON), Cairo, Egypt, Dec. 2019, pp. 103–110. doi:10.1109/MEPCON47431.2019.9008079